Acta of Bioengineering and Biomechanics
Vol. 26, No. 4, 2024

Original paper
DOI: 10.37190/ABB-02538-2024-02

Comparative analysis of orthopaedic scaffold fixation methods – a finite element study

ANITA GRYKO*, PIOTR PROCHOR

Institute of Biomedical Engineering, Faculty of Mechanical Engineering, Bialystok University of Technology, Białystok, Poland.

Purpose: Critical-size bone defects (CSBD) are a serious challenge in current orthopaedics. Natural healing processes are insufficient, leading to complications such as muscle atrophy, joint stiffness, impaired limb function and reduced quality of life. Currently used autologous or allogeneic bone grafts have disadvantages, such as long surgery time, secondary injuries and immunological reactions. A promising alternative in the treatment of CSBD is the use of a scaffold. The key element of the effective use of scaffolds is their proper anchoring in the bone defect. The article presents numerical analyses of the effectiveness of selected anchoring methods of the scaffold in the bone. *Methods*: Scaffolds were placed in a 60 mm long CSBDs. Four methods of anchoring the scaffold in the bone were selected: locking plate, external ring, intramedullary nail and double anti-rotation wedge. A simulation of the forces generated during the entire gait cycle was performed. The parameters obtained were: Huber Mises Hencky (HMH) max stress, strain energy density (SED), sliding distance, frictional stress and bone-scaffold gap. *Results*: Based on the conducted research, it was determined that the most effective of the evaluated solutions, in terms of load transfer, were the use of external ring or double anti-rotation wedge. *Conclusions*: The conducted research confirm that in the treatment of CSBD, an effective solution is the use of a scaffold, which effectiveness can be improved with appropriate anchoring method.

Key words: *critical-size bone defects, scaffold, fixation methods, orthopaedic treatment, gait cycle, finite element analysis*

1. Introduction

Fast recovery after bone damage is crucial to minimise fatality and ensure sufficient quality of life [20], [35]. Although the bone has the ability to heal itself, critical-size bone defects (CSBDs) hinder the natural healing process and do not allow for complete healing. CSBD is defined as bone loss greater than one-and-a-half long bone diameter or greater than one-fifth to one-fourth of the long bone length [19], [49]. The main causes of CSBDs are trauma, tumour resection, developmental deformities, infections, mechanical damage, diseases, cancer mutations and delayed union of long bones [19]. CSBDs may lead to further complications, such as muscle atrophy, joint stiffness, impaired limb function or reduced quality of life [49]. Treatment of CSBD is mostly based on the use of autologous or allogeneic bone grafts [19]. The main disadvantages of autologous bone grafts, which are currently considered the gold standard in CSBD repair, include: long surgery time, severe secondary injuries and limited number of donor sites [12]. Problems with allogeneic transplants result from the immune response, which affects the vascularisation and cellularity of the graft [45]. External and internal structures (such as locking plate or outer rings) are also used for stabilisation, which, despite their widespread use, have their drawbacks, such as disruption of the load transfer or the accumulation of stress at the anchorage point in the bone tissue [31].

* Corresponding author: Anita Gryko, Institute of Biomedical Engineering, Faculty of Mechanical Engineering, Bialystok University of Technology, Białystok, Poland. E-mail: anita.gryko@sd.pb.edu.pl
Received: October 28th, 2024
Accepted for publication: December 19th, 2024

A promising alternative in the treatment of CSBD is the use of a relatively new type of implant, which is scaffold [3], [19]. By definition, a scaffold is a porous structure, which provides temporary or permanent mechanical integrity at the site of tissue damage until it regenerates and restores its biomechanical functionality [9]. Individually adjusted scaffolds usually have inhomogeneous geometry [46] and appropriate porosity, which enable cell growth and proliferation, supply of nutrients and production of intercellular matrix [29]. The use of coatings on scaffolds additionally increases their functionality [15].

A properly designed scaffold structure allows for transferring loads from one bone fragment to another, which cannot be achieved using conventional treatment methods [49]. Currently, researchers are trying to develop scaffolds further, using various research methods [43]. Their main goal is to determine the optimal mechanical properties that will allow obtaining the highest possible functionality of scaffolds [5].

An important aspect of the effectiveness of bone reconstruction using scaffolds is their stable attachment to the bone tissue [21]. This process, called anchoring, plays a key role in providing adequate support for the growing bone tissue [38] and minimising the risk of implant displacement [13]. Effective anchoring of scaffolds in the bone provides not only mechanical stability, but also enables integration with the surrounding tissues, which contributes to effective bone healing and reconstruction [38]. Therefore, the development of methods and techniques for anchoring scaffolds is an important aspect in the further development of reconstructive treatment of CSBD.

This issue is relatively new, but the researches on the restoring bone continuity with the use of scaffolds are eagerly undertaken with the use of numerical [10], [27] or experimental methods [36], [42]. Numerical methods allow conducting research in simulated environment as well as easy monitoring computational errors and adjusting research parameters [8], which is often impossible with the use of experimental study.

Coquim et al. [10] performed a numerical analysis of intact bone, without defects and 8 different combinations of bone fixation using bone struts. They found that according to the traditional "high stiffness" criterion, fixation with a lateral metal plate and a medial bone strut is most functional, whereas according to the modern "low stiffness" criterion, it is more preferable to use only the lateral plate, even though this generates higher stresses that may exceed the bone strength.

Lu et al. [27] conducted research on bone structures with bone loss and 4 cases of bone union. They observed that bone fixation using a lateral plate and a medial bone strut provides the highest stiffness. However, while the lateral plate promotes secondary fracture healing, it also causes generating higher stresses.

Yang et al. [42] conducted a study to evaluate the effectiveness of scaffolds in the treatment of very large bone defects. The study was performed on a new model of metatarsal fractures in sheep that were stabilised with an intramedullary nail. They found out that the use of an osteoinductive scaffold effectively treats very large bone defects, ensuring bone regeneration and mechanical stability.

Park et al. [36] performed limb-sparing surgery using 3D printed implants for a patient with bone cancer, which resembled an outer ring. In this case again, the study proved that personalised implant significantly improves bone and soft tissue integration, suggesting high effectiveness in the treatment of large bone defects.

The cited research refers to bone fixation methods and the use of scaffolds for bone reconstruction. Numerical analyses have shown that a lateral plate with a medial bone support provides high stiffness, but the use of only a lateral plate is preferred to obtain lower stiffness despite higher stresses. Studies over bone loss have proved that bone strut with side plates also increase generated stresses. Osteoinductive scaffolds were effective in CSBDs, promoting regeneration and stability. Customised 3D printed implants have improved bone and soft tissue integration, showing promising results in the treatment of CSBDs.

Currently, the conducted researches so far proven that scaffolds are a better solution for filling bone defects. However, there is no clear indication or comparative assessment of the their anchoring methods. Therefore, the aim of this article was to compare various methods of anchoring scaffolds in bone tissue, with particular emphasis on their impact on Huber–Mises–Hencky's (HMH) stress, strain energy density (SED), sliding distance, frictional stress and bone--scaffold gap. These parameters were selected as key indicators of biomechanical stability and bone healing potential, which is confirmed in the literature [32], [37]. HMH stress and SED allow to assess the efficiency of load transfer and bone remodelling processes, while sliding distance, frictional stress and bone--scaffold gap refer to the mechanical stability of the implant and the potential risk of its loosening. Such comparison will allow for a better understanding of the advantages and limitations of individual methods, which will contribute to the optimisation of treatment methods of CSBD.

2. Materials and methods

2.1. CAD models

Bone model generation was carried out using 3D Slicer software with the use of its free database. The study used 442 CT images, every 1.5 mm, of the left femur of a 44-year-old man (mass = 85 kg, height = 185 cm). A threshold range of 226 to 1937 HU for initial bone tissue segmentation. Areas where the model was discontinuous required manual post-processing to, among other tasks, separate bone tissue from artifacts. The model was subsequently smoothed with a smoothing factor of 0.7. The final model was saved in .stl format and imported into SolidWorks 2021 SP 4.1 (Dassault Systèmes) to create CAD models. These models were then employed in further analyses using the finite element method. The effectiveness of this model was confirmed in other studies conducted by the authors [17]. This study included a CSBD length of 60 mm, located at a distance of 160 mm measured from the femur head. Selected defect parameters are often included in the literature and used in various numerical studies [27]. A scaffold was placed in the defect and various methods of anchoring it in the bone were used. The bone–implant schematic with dimensions is presented in Fig. 1.

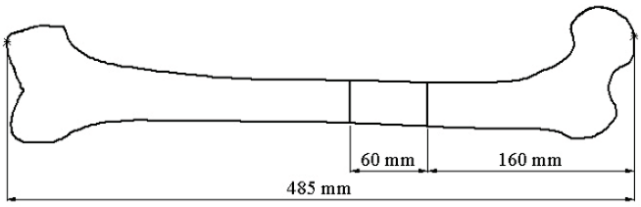

Fig. 1. Dimensions of the bone-implant model used in the study

In the study, 4 osteosynthesis methods were used, which are most often used in clinical practice [26], [36], [39], [42], [48]: 1 – locking plate, 2 – ring, 3 – intramedullary nail, 4 – double anti-rotation wedge. In all cases, the scaffold geometry was determined on the basis of the removed bone fragment. The diameter of the scaffold was adjusted to the anatomical dimensions of the bone shaft, to exactly fit the removed fragment.

On the basis of solutions available in the literature [26], [36], [39], [42], [48], 4 structures used as scaffold stabilisation method were modelled. The methods used to stabilize the scaffolds have been used in clinical conditions. In the first method of scaffold stabilisation in the bone (Fig. 2a), the commercially available DePuy Synthes Trauma Locking Compression Plate (LCP) system with 6 holes, 160 mm long and 15 mm wide, was used in combination with the scaffold. Additionally, to anchor locking plate, 6 self-tapping locking screws ∅ 4.5 (l = 22 mm) were used, 3 on the

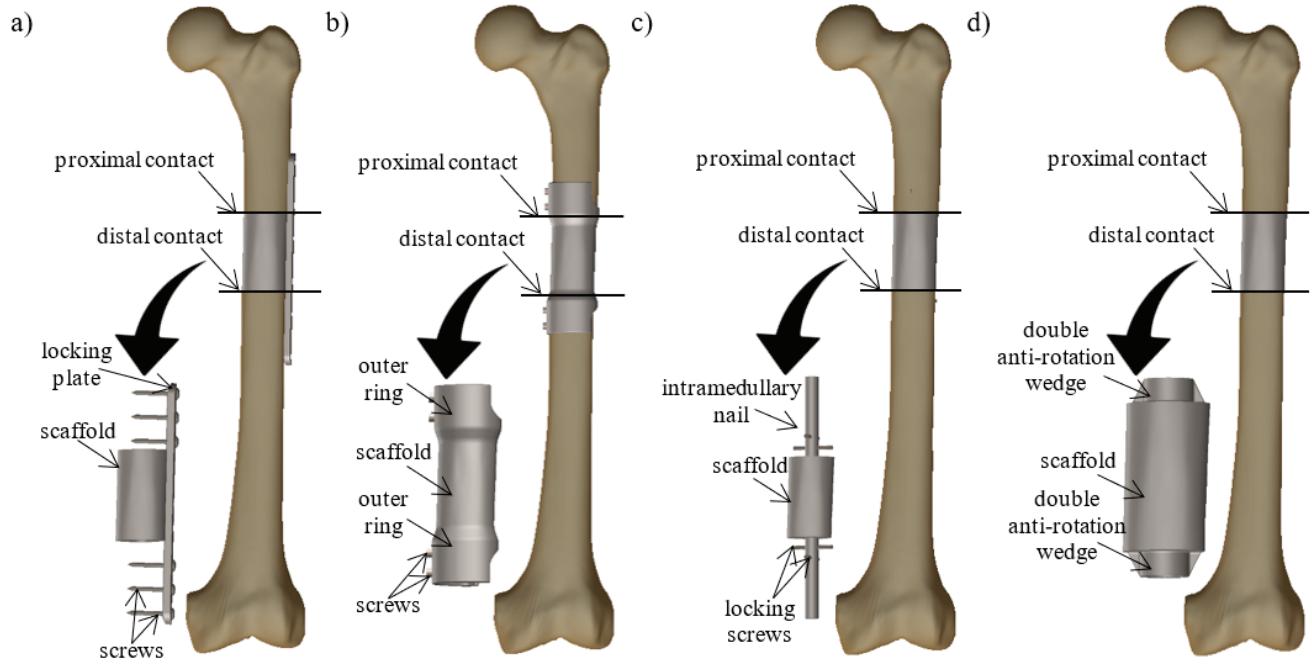

Fig. 2. Bone stabilisation methods used in the study: a) method 1 – locking plate, b) method 2 – outer ring, c) method 3 – intramedullary nail, d) method 4 – double anti-rotation wedge

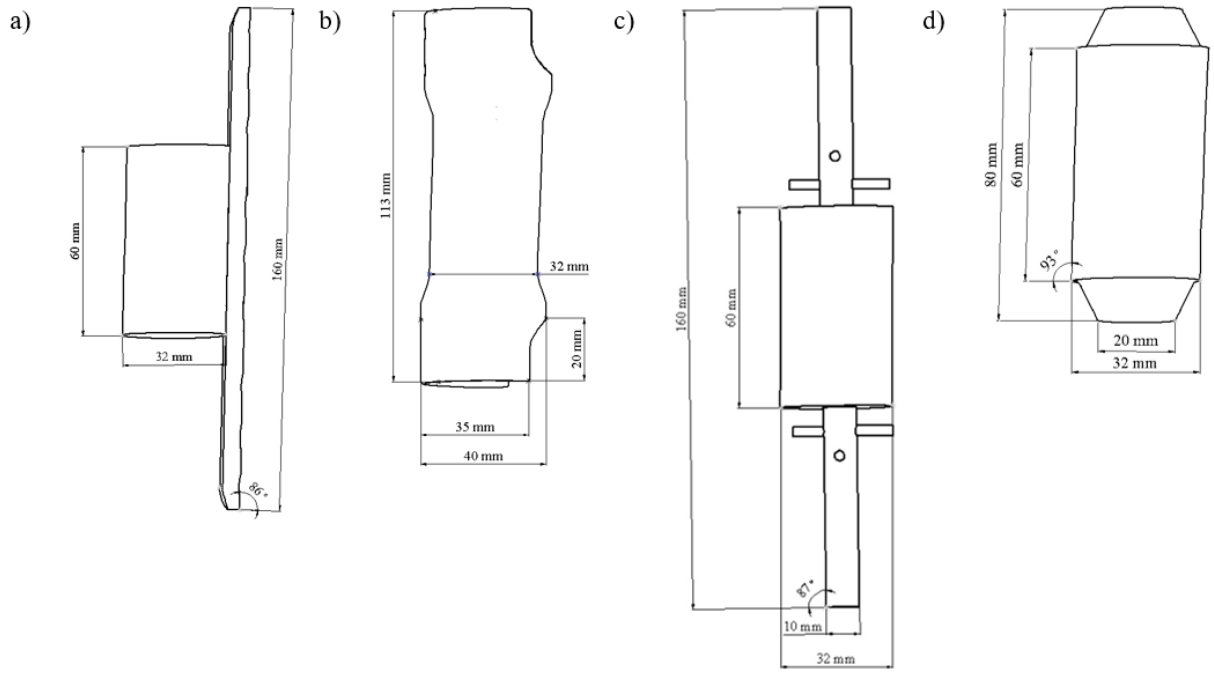

Fig. 3. Overall dimensions of scaffolds with anchoring elements in individual methods: a) method 1 – locking plate, b) method 2 – outer ring, c) method 3 – intramedullary nail, d) method 4 – double anti-rotation wedge

proximal and 3 on the distal side of the bone [39]. In the second method (Fig. 2b), the scaffold was attached to the bone through the outer ring and with the use of 4 self-tapping locking screws ∅ 4.5 (l = 16 mm) on each side, 2 on the proximal and 2 on the distal [36]. In the third method (Fig. 2c), intramedullary stabilisation was used to anchor the scaffold, which is generally recommended for attaching structures in the diaphysis area. Additionally, 2 locking screws on the proximal and 2 on the distal side were used [26]. In the fourth method (Fig. 2d), double anti-rotation wedge was modelled, which effectiveness was proved in several studies [42], [48]. In each stabilisation method, sliding distance, frictional stress and gap have been evaluated for proximal and distal contacts between implant and bone parts. In numerical analyses, the geometry of the screws was simplified, omitting the thread while maintaining the general dimensions. The overall dimensions of structures used in each method are presented in Fig. 3.

2.2. FE models

ANSYS Mechanical 2020 R1 software (ANSYS, Inc.) was used to conduct numerical studies. Isotropic and homogeneous mechanical properties of bone tissues were assumed. SS 316L and Ti6Al4V material properties were considered for anchoring elements and scaffolds respectively. However, in the case of scaffolds, effective Young's modulus of a scaffold with a porosity of 40% was considered in order to appropriately simulate the influence of porosity on structure's stiffness. This porosity was proven by the authors to have the highest biomechanical functionality in one of the previous studies [18]. Material properties used to conduct numerical study are listed in Table 1.

The models were discretised using 10-node Solid187 tetrahedral elements [2]. The maximum edge length of the finite element was set on 5 mm. In contact zones, mesh was additionally refined by lowering the finite

Table 1. Material properties used in the study

	Density [g/cm^3]	Young's Modulus [GPa]	Poisson's Ratio	Effective Young's Modulus [GPa]
Cortical bone	1.74 [22]	20.00 [22]	0.30 [22]	–
Cancellous bone	0.64 [1]	0.40 [1]	0.30 [1]	–
Anchoring elements (SS 316L)	7.85 [24]	190.00 [24]	0.30 [24]	–
Scaffold 40% porosity (Ti6Al4V)	4.50 [7]	–	0.33 [7]	30.00 [18]

element edge length to 1 mm. Discretisation quality was controlled with the use of Jacobian coefficient. According to the literature, to maintain appropriate quality of mesh, the minimum value of the Jacobian coefficient should be above 0.4 [32]. All analysed finite element models were characterised by a Jacobian ratio above 0.4. Additionally, in order to confirm that the appropriate mesh quality was obtained, a 5% mesh convergence test was also performed for max. HMH stress – the mesh was refined globally and locally until the results were not changed by more than 5%. Models consisted of 85 ± 10 thousand elements. An example of the generated mesh and the distribution of the Jacobian coefficient on one of the generated models is presented in Fig. 4.

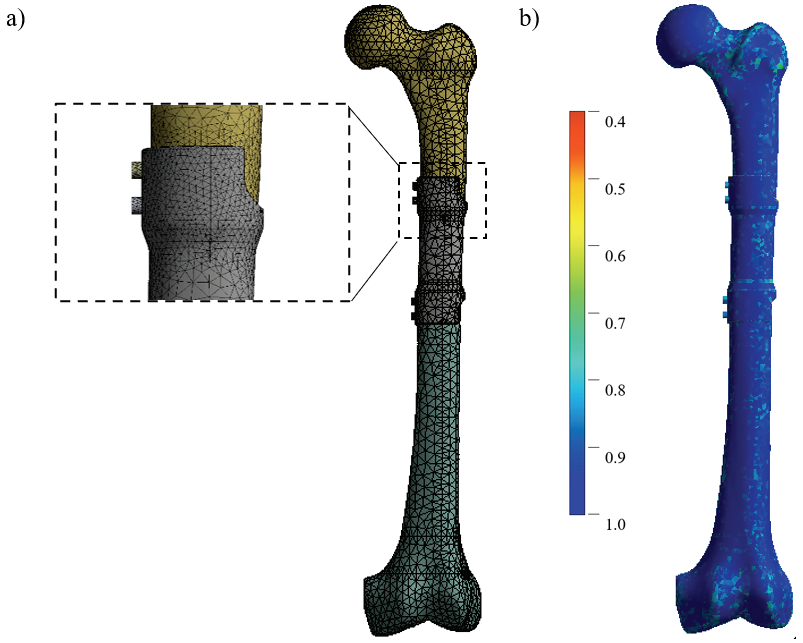

Fig. 4. Exemplary model after discretisation: a) mesh, b) Jacobian ratio distribution

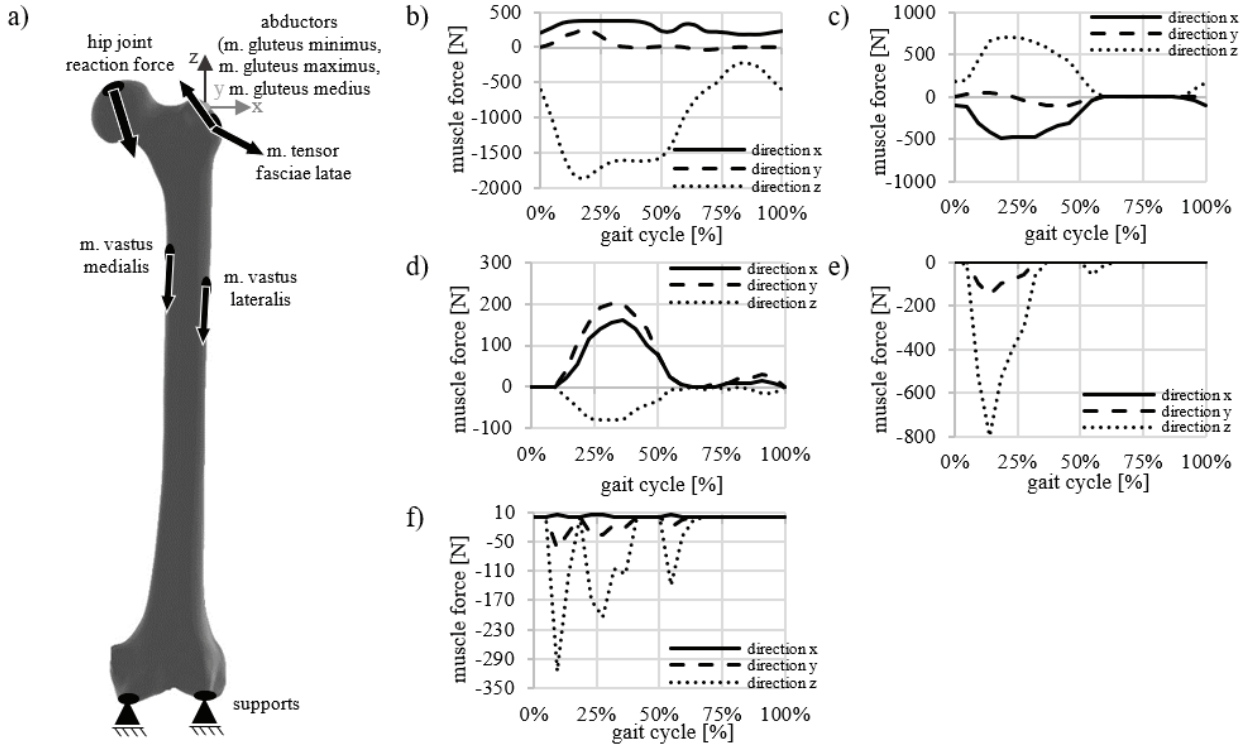

Fig. 5. Boundary conditions and forces values considered in the study: a) visualisation, b) hip joint reaction force, c) abductors, d) tensor fascia latae, e) vastus lateralis, f) vastus medialis

The following types of contacts have been established: frictional contact with a coefficient of 0.3 between bone and scaffold as well as scaffold and screws [27]. Despite the geometrical simplifications used, the contact geometry correction was assumed with bolt thread of the following parameters: mean pitch diameter of 4.013 mm, pitch distance of 0.75 mm and thread angle of 60°.

All forces acting on the femur during the gait cycle healthy man were taken into account [4]: hip joint reaction force and forces generated by selected muscles (gluteus medius, gluteus maximus, gluteus medius, tensor fascia lata, vastus lateralis, vastus medialis). Supports and applied forces are presented in Fig. 5.

3. Results

In order to assess the effectiveness of load transfer, the results obtained for each of the analysed anchoring method were compared with the results obtained for the intact femur.

The analysed parameters included max. HMH stress, SED, sliding distance, frictional stress and bone-scaffold gap. HMH stress and SED are biological indicators that enable the assessment of the bone remodelling process and the efficiency of load transfer through bone [32]. Sliding distance, frictional stress and bone-scaffold gap allow to assess the functioning of the scaffold-bone

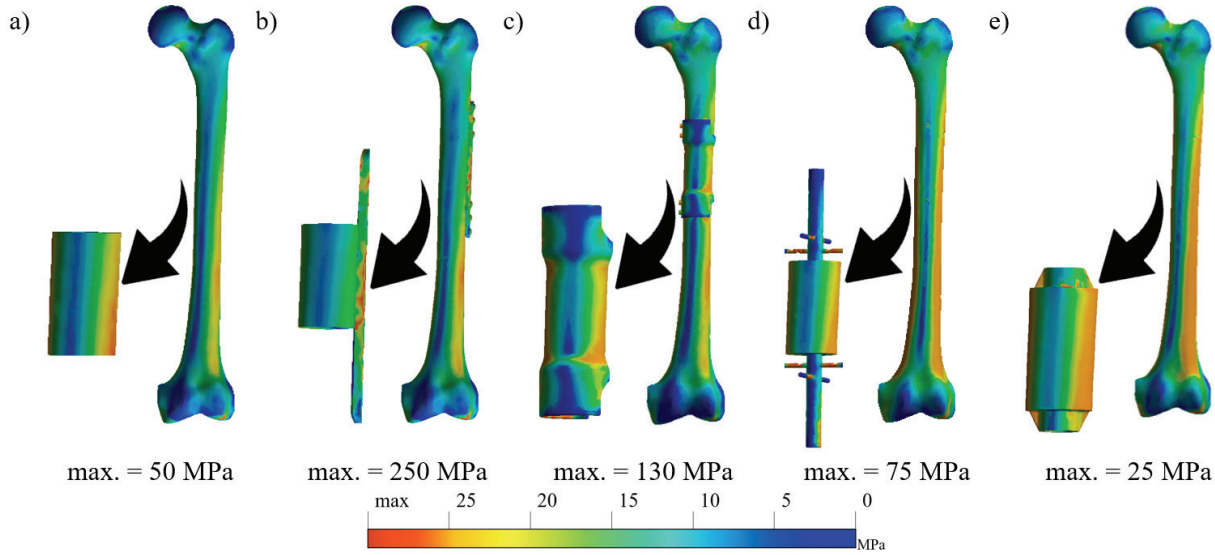

Fig. 6. HMH stress distribution for 20% of the gait cycle: a) intact femur, b) method 1 – locking plate, c) method 2 – outer ring, d) method 3 – intramedullary nail, e) method 4 – double anti-rotation wedge

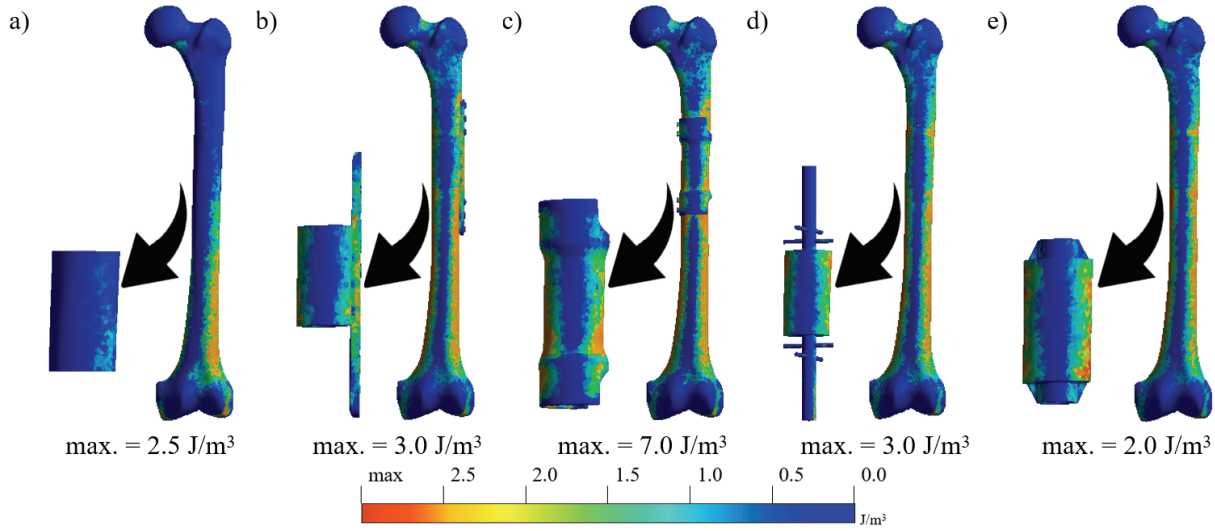

Fig. 7. SED distribution: a) intact femur, b) method 1 – locking plate, c) method 2 – outer ring, d) method 3 – intramedullary nail, e) method 4 – double anti-rotation wedge

connection, which is crucial for the long-term efficiency of implants [37].

HMH stress and SED distribution for the intact femur and each of the analysed anchoring methods are presented in Figs. 6 and 7. The maps were generated for approximately 20% of the gait cycle (it was a moment of obtaining the highest values of analysed parameters). HMH stress and SED results for the lateral and isometric views have been included in Supplementatry Materials (at the end of

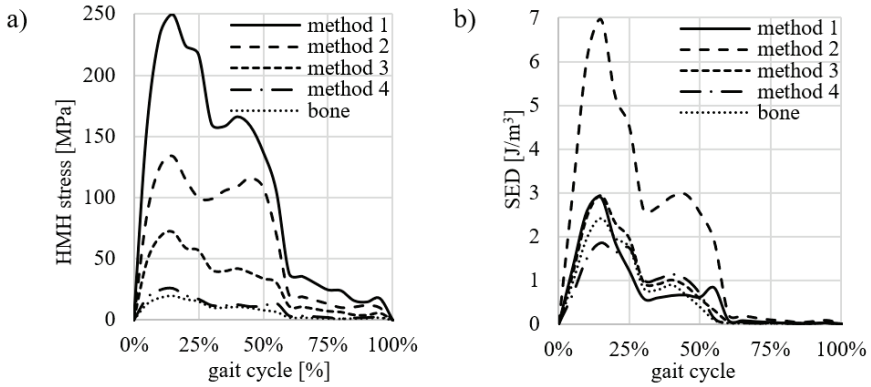

Fig. 8. Max. values obtained for full gait cycle: a) HMH stress, b) SED

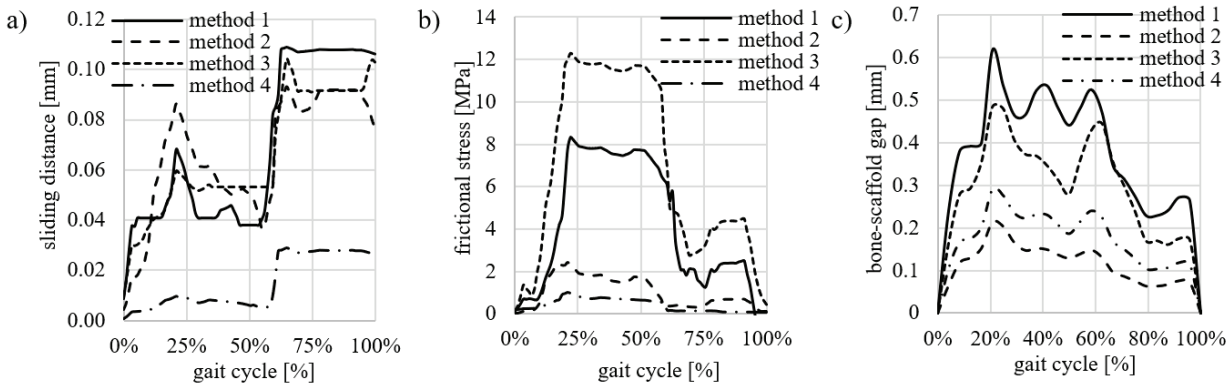

Fig. 9. Max. values obtained for full gait cycle: a) sliding distance, b) frictional stress, c) bone-scaffold

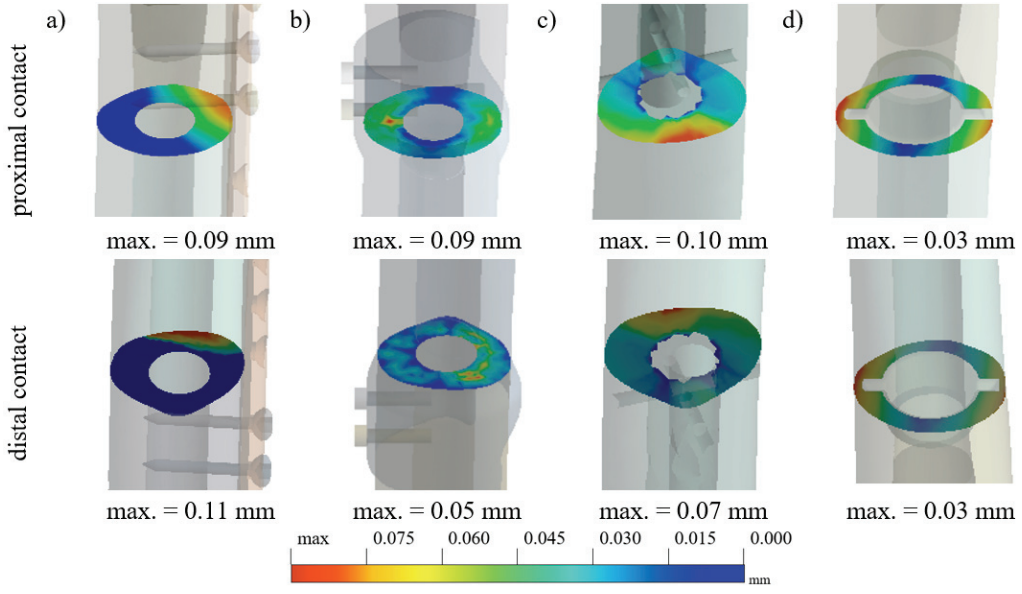

Fig. 10. Sliding distance: a) method 1 – locking plate, b) method 2 – outer ring, c) method 3 – intramedullary nail, d) method 4 – double anti-rotation wedge

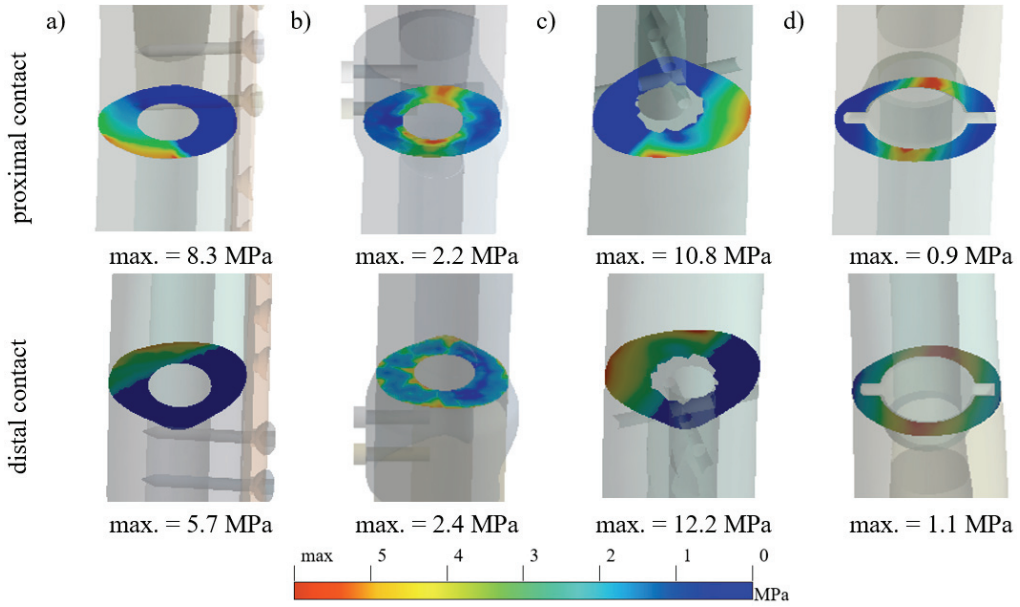

Fig. 11. Frictional stress: a) method 1 – locking plate, b) method 2 – outer ring, c) method 3 – intramedullary nail, d) method 4 – double anti-rotation wedge

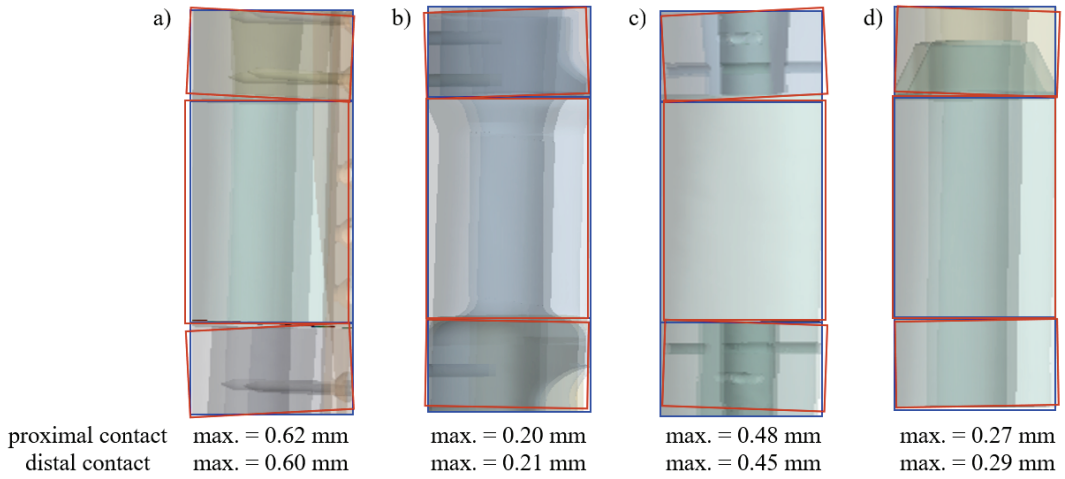

Fig. 12. Bone-scaffold gap (blue lines indicate undeformed model, while red deformed model): a) method 1 – locking plate, b) method 2 – outer ring, c) method 3 – intramedullary nail, d) method 4 – double anti-rotation wedge

the article) to increase the clarity of the results (Figs. S1–S4).

In order to compare the selected anchoring methods more precisely, values of max. HMH stress and SED are presented in Fig. 8, while max. sliding distance, frictional stress and bone-scaffold gap obtained for the full gait cycle are displayed in Fig. 9.

Sliding distance, frictional stress and bone-scaffold gap for the analysed anchoring methods are presented in Figs. 10–12. Sliding distance and frictional stress were determined for bone-scaffold frictional contacts. The bone-scaffold gap is presented as the distance in vertical direction created between bone fragments and scaffold: blue lines include undeformed model, while red deformed model.

4. Discussion

In the presented article, the authors numerically evaluated 4 different anchoring methods of scaffolds as CSBD treatment solution and restoring bone continuity. Scaffolds were anchored in the bone using locking plate (method 1), outer ring (method 2), intramedullary nail (method 3), and double anti-rotation wedge (method 4). The article provides analyses over max. HMH stress, SED, sliding distance, frictional stress and bone-scaffold gap, as key indicators of biomechanical stability and bone healing potential, which is confirmed in the literature [32], [37]. HMH stress and SED allow the assessment of the load transfer efficiency and bone remodel-

ling processes, with HMH stress referring to the risk of mechanical damage in both the bone and the implant, while SED is crucial in assessing the bone remodelling and healing process. Sliding distance, frictional stress and bone-scaffold gap refer to the mechanical stability of the implant and the potential risk of its loosening.

Stress distribution maps for the intact femur indicate the zones with the highest stresses (approx. 50 MPa), i.e., in the medial and lateral parts of the shaft, in the medial and lateral condyles and at the femoral neck. The lowest stresses (approx. 5 MPa) occur in the anterior and posterior parts of the shaft, the anterior and posterior parts of the distal epiphysis, the greater trochanter and femoral head. The data coincide with the values available in the literature [11]. When a critical-size bone defect occurs, the stress distribution severely changes due to different loads transfer. It also causes visible risk of stress-shielding [23] as a result of too high stiffness of implants used to restore bone continuity [10]. According to the literature, SED for an intact femur reaches threshold of around 0.2–2.4 J/m^3 [47], which coincides with the values obtained in the presented research. For methods 1 and 2, the stress of 250 MPa and 130 MPa and SED of 3 and 7 J/m^3 were obtained. The results obtained for locking plate coincide with those presented in the literature, where the maximum stress is in the range of 180–300 MPa [28]. The maximum stresses and SED for methods 3 and 4 were 75 and 25 MPa and 3 and 2 J/m^3. Literature values obtain by other authors in numerical studies, indicate that the maximum stresses for intramedullary stabilisation are in the range of 100 to 200 MPa [33]. The values closest to those of intact bone were obtained for method 4, while slightly higher values were obtained for method 3. The largest differences are noticeable for the other two anchoring methods, namely the locking plate and the external ring. Differences ranged from 100 to even 225 MPa. Methods 1, 3 and 4 provided SED values close to those of bone, with a maximum difference of 0.5 J/m^3. However, for method 2, the differences between the values for intact bone and the anchoring methods were much higher, reaching a maximum value of 7 J/m^3.

In some cases, there may be discrepancies between the results obtained by the authors and the results available in the literature [6], [34]. This is noticeable in method 2, which led to higher stress concentrations near the bone–implant contact surface. The reason may be the positioning of the anchoring element, which, due to its high stiffness, may lead to obtaining different results depending on the place where CSBD is located.

The SED values for method 4 are most similar to the values obtained for intact bone, which suggests the load transfer with this method reflects natural loads transfer through the bone.

It is worth noticing that, within a certain range of elastic deformations, higher values of HMH and SED are beneficial as they stimulate bone remodelling. However, it is important that these parameters do not exceed certain threshold, as this may lead to damages within bone structure.

At approximately 0–10% of the gait cycle (heel strike) stress and SED are low, but increase quickly as the foot moves into the next stage (foot flat) in which stress and SED reach one of the first maximums, which is related to the full load on the foot. At about 30–50% of the cycle (midstance) the stress and SED values decrease. Stress and SED start to increase for the second time and reach second maximum with toe off at approx. 50–60% of the gait cycle. Stress and SED decrease before entering the swing phase and retain their values for remaining 40% of the gait cycle. During that phase, stress and SED values are minimal as the limb is not loaded.

Loads during gait cycle also affect the sliding distance, frictional stress and bone-scaffold gap values. For the first and third parameter, as a result of the transition of the foot from the support phase to the transfer phase (approx. 60% of the cycle), the values increase, while for the second one, on the contrary, decrease significantly. At 20% of the gait cycle, the sliding distance reaches its peak for the stance phase. At the moment of transition from the stance phase to the swing phase (approx. 60% of the cycle), the values increase again and remain high until the full cycle ends. Max. sliding distance values in method 1 were obtained for the distal contact (0.11 mm), in method 2 for the proximal contact (0.09 mm), in method 3 for the proximal contact (0.10 mm) and in method 4 for the proximal and distal contacts the values were the same (0.03 mm). The values obtained by the authors are within the range of values available in the literature, which is 0.001–0.720 mm, depending on the performed activity or the type of implant [14], [37]. Moreover, according to the literature based on clinical studies, the sliding distance at the interface between the implant and the bone should be greater than 0.028 mm but cannot exceed 0.150 mm to guarantee effective bone growth [16], [41]. Sliding distance above this range may lead to loosening of the implant and the growth of fibrous tissue at the bone-implant interface, thus hindering proper implant fixation [16], [41]. The values obtained by the authors are within the range given in the literature. For frictional stress, the values also start to increase with foot flat (approx. 20% of the cycle). The maximum values of frictional stress in the method 1

were obtained for the proximal contact (8.3 MPa), in method 2 – for the distal contact (2.4 MPa), in method 3 – for the distal contact (12.2 MPa), in method 4 – for the distal contact (1.1 MPa) and remain similar until the support phase ends, while with the start of swing phase they drop significantly.

A similar tendency as in frictional stress can also be observed for scaffold-bone gaps. When foot flat starts, the values reach their maximum, which in method 1 were obtained for the proximal contact (0.62 mm), in method 2 for the distal contact (0.21 mm), in method 3 for the proximal contact (0.48 mm) and in method 4 for the distal contact (0.29 mm). At the moment of entering the swing phase, the values start to decrease. According to the literature on bone fractures, for the fracture gap to heal, it must be smaller than 0.8 mm [30]. For the anchoring methods analysed, this value was not exceeded, which may indicate that the fragments will heal. Frictional stress and gap behave opposite to sliding distance – when sliding distance increases, frictional stress and gap decreases. The highest values of sliding distance and gap were recorded for method 1, and frictional stress for method 3. The lowest values of sliding distance and frictional stress were obtained for method 4, and the gap for method 2. It is important that when using the selected anchoring method, the tested parameters are as low as possible to eliminate excessive movements of the implant in the vertical and transverse directions, which could contribute to joint instability. For the locking plate (in the distal contact), the external ring (in the proximal contact) and the intramedullary nail (in the proximal contact), the solution could be to use additional stabilising screws to increase their biomechanical efficiency.

Sources of model validation are based on clinical trials, animal experiments and previous numerical models. This approach increases the credibility of the results and allows them to be better related to clinical practice [25], [40].

The research results have presented that the methods using external ring and double anti-rotation wedge are the most optimal in terms of load transfer. These methods promote the integration of the implant with the bone, i.a., through the appropriate level of SED, minimisation of stress concentration and preventing creation of fibrous tissue.

5. Conclusions

The conducted research confirm that the use of a scaffold with appropriate anchoring method is an effective solution in the treatment of CSBD. The use of an external ring and double anti-rotation wedge are particularly promising. The indicated geometries provide additional stability and better integration with bone tissue. The use of an external ring or double anti-rotation wedge may also reduce the risk of scaffold loosening, which is important to ensure lasting treatment results. Further research should focus on optimising these anchoring methods in order to improve the effectiveness of using scaffolds as a method of restoring bone continuity in CSBDs.

Acknowledgements

The research was funded by Ministry of Education and Science, Poland as a part of projects WI/WM-IIB/6/2023 and WI/WM-IIB/5/2023.

Role and contribution of each co-author in the preparation of the manuscript

A. Preparation of the research program: Anita Gryko, Piotr Prochor;
B. Execution of the research: Anita Gryko, Piotr Prochor;
C. Statistical analysis: Anita Gryko, Piotr Prochor;
D. Interpretation of data: Anita Gryko, Piotr Prochor;
E. Preparation of the manuscript: Anita Gryko, Piotr Prochor;
F. Obtaining funding: Anita Gryko, Piotr Prochor.

References

[1] ALKHATIB S.E., MEHBOOB H., TARLOCHAN F., *Finite element analysis of porous titanium alloy hip stem to evaluate the biomechanical performance during walking and stair climbing*, J. Bionic. Eng., 2019, 16, 1103–1115, DOI: 10.1007/s42235-019-0122-4.

[2] ANDREAUS U.A., COLLOCA M., TOSCANO A., *Mechanical behaviour of a prosthesized human femur: a comparative analysis between walking and stair climbing by using the finite element method*, Biophysics and Bioengineering Letters, 2008, 1 (3).

[3] ANTONOWICZ M., BRZEZIŃSKA K., WALKE W., TARATUTA A., PAWLIK M., *Biodegradable scaffolds for bone defect treatment*, Acta Bioeng. Biomech., 2023, 25 (3), 1–14, DOI: 10.37190/ABB-02318-2023-03.

[4] BEHRENS B.A., NOLTE I., WEFSTAEDT P., STUKENBORG-COLSMAN C., BOUGUECHA A., *Numerical investigations on the strain-adaptive bone remodelling in the periprosthetic femur: influence of the boundary conditions*, Biomed. Eng. Online, 2009, 8, 1–9, DOI: 10.1186/1475-925X-8-7.

[5] BIGHAM A., AGHAJANIAN A.H., SAUDI A., RAFIENIA M., *Hierarchical porous Mg_2SiO_4-$CoFe_2O_4$ nanomagnetic scaffold for bone cancer therapy and regeneration: surface modification and in vitro studies*, Mater Sci. Eng. C., 2020, 109, 110579, DOI: 10.1016/j.msec.2019.110579.

[6] CALVO-GALLEGO J.L., GUTIÉRREZ-MILLÁN F., OJEDA J., PÉREZ M.Á., MARTÍNEZ-REINA J., *The correlation between bone density and mechanical variables in bone remodelling models: Insights from a case study corresponding to the femur of a healthy adult*, Mathematics, 2022, 10 (18), 3367, DOI: 10.3390/math10183367.

[7] CAPITANU L., FLORESCU V., BADITA L.L., *New concept in durability improvement of hip total joint endoprostheses*, Acta Bioeng. Biomech., 2014, 16 (1), 75–82, DOI: 10.5277/abb140110.

[8] CHABAROVA O., SELIVONEC J., *Virtual modelling the impact of torsional loading on osteoporotic vertebrae buckling*, Acta Bioeng. Biomech., 2024, 26 (1), 1–10, DOI: 10.37190/ABB-02392-2024-03.

[9] CHAUDHARI A.A., VIG K., BAGANIZI D.R., SAHU R., DIXIT S., DENNIS V., SINGH S.R., PILLAI S.R., *Future prospects for scaffolding methods and biomaterials in skin tissue engineering: a review*, Int. J. Mol. Sci., 2016, 17 (12), 1974, DOI: 10.3390/ijms17121974.

[10] COQUIM J., CLEMENZI J., SALAHI M., SHERIF A., TAVAKKOLI AVVAL P., SHAH S., SCHEMITSCH E.H., BAGHERI Z.S., BOUGHERARA H., ZDERO R., *Biomechanical analysis using FEA and experiments of metal plate and bone strut repair of a femur midshaft segmental defect*, Biomed. Res. Int., 2018, (1), 4650308, DOI: 10.1155/2018/4650308.

[11] FOX M.J., SCARVELL J.M., SMITH P.N., KALYANASUNDARAM S., STACHURSKI Z.H., *Lateral drill holes decrease strength of the femur: an observational study using finite element and experimental analyses*, J. Orthop. Surg. Res., 2013, 8, 1–8, DOI: 10.1186/1749-799X-8-29.

[12] FU Q., SAIZ E., RAHAMAN M.N., TOMSIA A.P., *Toward strong and tough glass and ceramic scaffolds for bone repair*, Adv. Funct. Mater., 2013, 23 (44), 5461–5476, DOI: 10.1002/adfm.201301121.

[13] GAO S.S., ZHANG Y.R., ZHU Z.L., YU H.Y., *Micromotions and combined damages at the dental implant/bone interface*, Int. J. Oral. Sci., 2012, 4 (4), 182–188, DOI: 10.1038/ijos.2012.68.

[14] GAO Y., CHAI W., WANG L., WANG M., JIN Z., *Effect of friction and clearance on kinematics and contact mechanics of dual mobility hip implant*, Proc. Inst. Mech. Eng. Part H: J. Eng. Med., 2016, 230 (1), 39–49, DOI: 10.1177/0954411915617198.

[15] GOLDSZTAJN K., GODZIERZ M., HERCOG A., WŁADOWSKI M., JAWORSKA J., JELONEK K., WOŹNIAK A., KAJZER W., ORŁOWSKA A., SZEWCZENKO J., *Properties of biodegradable polymer coatings with hydroxyapatite on a titanium alloy substrate*, Acta Bioeng. Biomech., 2024, 26 (1), 1–2, DOI: 10.37190/ABB-02351-2023-03.

[16] GORGULUARSLAN R.M., GANDHI U.N., SONG Y., CHOI S.K., *An improved lattice structure design optimization framework considering additive manufacturing constraints*, Rapid Prototyp J., 2017, 23 (2), 305–319, DOI: 10.1108/RPJ-10-2015-0139.

[17] GRYKO A., PROCHOR P., *Numerical evaluation of scaffolds as a method to restore continuity of a long bone*, J. Comput. Sci., 2024, 79, 102314, DOI: 10.1016/j.jocs.2024.102314.

[18] GRYKO A., PROCHOR P., SAJEWICZ E., *Finite element analysis of the influence of porosity and pore geometry on mechanical properties of orthopaedic scaffolds*, J. Mech. Behav. Biomed. Mater., 2022, 132, 105275, DOI: 10.1016/j.jmbbm.2022.105275.

[19] HAN J., WU J., XIANG X., XIE L., CHEN R., LI L., MA K., SUN Q., YANG R., HUANG T., TONG L., ZHU L., WANG H., WEN C., ZHAO Y., WANG J., *Biodegradable BBG/PCL composite scaffolds fabricated by selective laser sintering for directed regeneration of critical-sized bone defects*, Mater. Des., 2023, 225, 111543, DOI: 10.1016/j.matdes.2022.111543.

[20] HATA K., ISHIDO Y., FUKUDOME K., KIYAMA R., KAWADA M., NISHI T., NAKATSUJI S., YONE K., *Effect of alteration in hip joint alignment following total hip arthroplasty on hip joint contact force during gait*, Acta Bioeng. Biomech., 2023, 25 (3), 1–10, DOI: 10.37190/ABB-02284-2023-02.

[21] HEINECKE M., LAYHER F., MATZIOLIS G., *Anchoring of a kinked uncemented femoral stem after preparation with a straight or a kinked reamer*, Orthop. Surg., 2019, 11 (4), 705–711, DOI: 10.1111/os.12490.

[22] HERRERA A., PANISELLO J.J., IBARZ E., CEGOÑINO J., PUÉRTOLAS J.A., GRACIA L., *Long-term study of bone remodelling after femoral stem: a comparison between dexa and finite element simulation*, J. Biomech., 2007, 40 (16), 3615–3625, DOI: 10.1016/j.jbiomech.2007.06.008.

[23] JOSHI M.G., ADVANI S.G., MILLER F., SANTARE M.H., *Analysis of a femoral hip prosthesis designed to reduce stress shielding*, J. Biomech., 2000, 33 (12), 1655–1662, DOI: 10.1016/s0021-9290(00)00110-x.

[24] KUFFNER B.H.B., CAPELLATO P., RIBEIRO L.M.S., SACHS D., SILVA G., *Production and characterization of a 316L stainless steel/β-TCP biocomposite using the functionally graded materials (fgms) technique for dental and Orthopedic Applications*, Metals, 2021, 11 (12), 1923, DOI: 10.3390/met11121923.

[25] LI J., SUN Z., WEI X., TAN Q., HE X., *Effect of Structure on Osteogenesis of Bone Scaffold: Simulation Analysis Based on Mechanobiology and Animal Experiment Verification*, Bioeng., 2024, 11 (11), 1120, DOI: 10.3390/bioengineering11111120.

[26] LIU B., HOU G., YANG Z., LI X., ZHENG Y., WEN P., LIU Z., ZHOU F., TIAN Y., *Repair of critical diaphyseal defects of lower limbs by 3D printed porous Ti6Al4V scaffolds without additional bone grafting: a prospective clinical study*, J. Mater. Sci.: Mater. Med., 2022, 33 (9), 64, DOI: 10.1007/s10856-022-06685-0.

[27] LU J., WANG Q.Y., SHENG J.G., GUO S.C., TAO S.C., *A 3D-printed, personalized, biomechanics-specific beta-tricalcium phosphate bioceramic rod system: personalized treatment strategy for patients with femoral shaft non-union based on finite element analysis*, BMC Musculoskelet. Disord., 2020, 21, 1–9, DOI: 10.1186/s12891-020-03465-1.

[28] LUO C., WU X.D., WAN Y., LIAO J., CHENG Q., TIAN M., BAI Z., HUANG W., *Femoral stress changes after total hip arthroplasty with the ribbed prosthesis: a finite element analysis*, Biomed. Res. Int., 2020, 2020 (1), 6783936, DOI: 10.1155/2020/6783936.

[29] MAJUMDER S., GUPTA A., DAS A., BARUI A., DAS M., CHOWDHURY A.R., *Comparing the bone regeneration potential between a trabecular bone and a porous scaffold through osteoblast migration and differentiation: a multiscale approach*, Int. J. Numer. Method. Biomed. Eng., 2024, e3821, DOI: 10.1002/cnm.3821.

[30] MARSELL R., EINHORN T.A., *The biology of fracture healing*, Injury, 2011, 42 (6), 551–555, DOI: 10.1016/j.injury.2011.03.031.

[31] MINI D., REYNOLDS K.J., TAYLOR M., *Assessing screw length impact on bone strain in proximal humerus fracture fixation via surrogate modelling*, Int. J. Numer. Method. Biomed. Eng., 2024, e3840, DOI: 10.1002/cnm.3840.

[32] MUKHERJEE N., MAKEM J.E., FOGG H.J., *A 3D constrained optimization smoother to post-process quadrilateral meshes for body-in-white*, Procedia Eng., 2016, 163, 262–275, DOI: 10.1016/j.proeng.2016.11.057.

[33] NIE S., LI J., LI M., HAO M., WANG K., XIONG Y., GAN X., ZHANG L., TANG P., *Finite Element Analysis of a Novel Cephalomedullary Nail for Restricted Sliding to Reduce*

Risk of Implant Failure in Unstable Intertrochanteric Fractures, Orthop. Surg., 2022, 14 (11), 3009–3018, DOI: 10.1111/os.13497.

[34] OLIVEIRA H., BRIZUELA VELASCO A., RÍOS-SANTOS J.V., SÁNCHEZ LASHERAS F., LEMOS B.F., GIL F.J., CARVALHO A., HERRERO-CLIMENT M., *Effect of different implant designs on strain and stress distribution under non-axial loading: A three-dimensional finite element analysis*, Int. J. Environ. Res. Public Health, 2020, 17 (13), 4738, DOI: 10.3390/ijerph17134738.

[35] ONO K., INOUE Y., YAMASAKI R., TANAKA S., TANAKA R., *The effect of using walking poles on the spatiotemporal gait parameters in patients who underwent surgery for hip fractures*, Acta Bioeng. Biomech., 2024, 26 (2), 1–9, DOI: 10.37190/ABB-02450-2024-02.

[36] PARK J.W., SONG C.A., KANG H.G., KIM J.H., LIM K.M., KIM H.S., *Integration of a three-dimensional-printed titanium implant in human tissues: case study*, Appl. Sci., 2020, 10 (2), 553, DOI: 10.3390/app10020553.

[37] SOLIMAN M.M., CHOWDHURY M.E., ISLAM M.T., MUSHARAVATI F., MAHMUD S., HAFIZH M., AYARI M.A., KHANDAKAR A., ALAM M.K., NEZHAD E.Z., *Design and Performance Evaluation of a Novel Spiral Head-Stem Trunnion for Hip Implants Using Finite Element Analysis*, Materials, 2023, 16 (4), 1466, DOI: 10.3390/ma16041466.

[38] TURNBULL G., CLARKE J., PICARD F., RICHES P., JIA L., HAN F., SHU W., *3D bioactive composite scaffolds for bone tissue engineering*, Bioact. Mater., 2018, 3 (3), 278–314, DOI: 10.1016/j.bioactmat.2017.10.001.

[39] WANG X., WANG S., XU J., SUN D., SHEN J., XIE Z., *Antibiotic cement plate composite structure internal fixation after debridement of bone infection*, Sci. Rep., 2021, 11 (1), 16921, DOI: 10.1038/s41598-021-96522-1.

[40 WANG Y., WANG L., SORO N., LI Z., TETSWORTH K., ERBULUT D., *Bone Ingrowth Simulation within a Novel Microstructure Scaffold*, 3D Print Addit. Manuf., 2023, DOI: 10.1089/3dp.2023.0113.

[41] WENG S., LIN D., ZENG J., LIU J., ZHENG K., CHEN P., LIN C., LIN F., *Optimal sliding distance in femoral neck system for displaced femoral neck fractures: a retrospective cohort study*, J. Orthop. Surg. Res., 2024, 19 (1), 690, DOI: 10.1186/s13018-024-05190-0.

[42] YANG Y.P., LABUS K.M., GADOMSKI B.C., BRUYAS A., EASLEY J., NELSON B., PALMER R.H., MCGILVRAY K., REGAN D., PUTTLITZ C.M., STAHL A., LUI E., LI J., MOEINZADEH S., KIM S., MALONEY W., GARDNER M.J., *Osteoinductive 3D printed scaffold healed 5 cm segmental bone defects in the ovine metatarsus*, Sci. Rep., 2021, 11 (1), 6704, DOI: 10.1038/s41598-021-86210-5.

[43] YU J., XIA H., NI Q.Q., *A three-dimensional porous hydroxyapatite nanocomposite scaffold with shape memory effect for bone tissue engineering*, J. Mater. Sci., 2018, 53 (7), 4734–4744, DOI: 10.1007/s10853-017-1807-x.

[44] ZAWADZKA M., KOZŁOWSKA J., EJCHMAN-PAC E., HENRYKOWSKA G., LEWICKA M., *Analysis of functional efficiency and risk of falls in patients with different types of dementia-preliminary observations*, Ann. Agr. Env. Med., 2024, 31 (1), DOI: 10.26444/aaem/168787.

[45] ZHANG H., ZHOU Y., YU N., MA H., WANG K., LIU J., ZHANG W., CAI Z., HE Y., *Construction of vascularized tissue-engineered bone with polylysine-modified coral hydroxyapatite and a double cell-sheet complex to repair a large radius bone defect in rabbits*, Acta Biomater., 2019, 91, 82–98, DOI: 10.1016/j.actbio.2019.04.024.

[46] ZHANG J., ZHAO S., ZHU M., ZHU Y., ZHANG Y., LIU Z., ZHANG C., *3D-printed magnetic Fe_3O_4/MBG/PCL composite scaffolds with multifunctionality of bone regeneration, local anticancer drug delivery and hyperthermia*, J. Mater. Chem. B., 2014, 2 (43), 7583–7595, DOI: 10.1039/C4TB01063A.

[47] ZHANG Y., LUO Y., *Femoral bone mineral density distribution is dominantly regulated by strain energy density in remodeling*, Biomed. Eng., 2020, 31 (3), 179–190, DOI: 10.3233/BME-206000.

[48] ZHENG Y., HAN Q., LI D., SHENG F., SONG Z., WANG J., *Promotion of tendon growth into implant through pore-size design of a Ti-6Al-4V porous scaffold prepared by 3D printing*, Mater. Des., 2021, 197, 109219, DOI: 10.1016/j.matdes.2020. 109219.

[49] ZHU L., LUO D., LIU Y., *Effect of the nano/microscale structure of biomaterial scaffolds on bone regeneration*, Int. J. Oral. Sci., 2020, 12 (1), 6, DOI: 10.1038/s41368-020-0073-y.

Supplementary materials

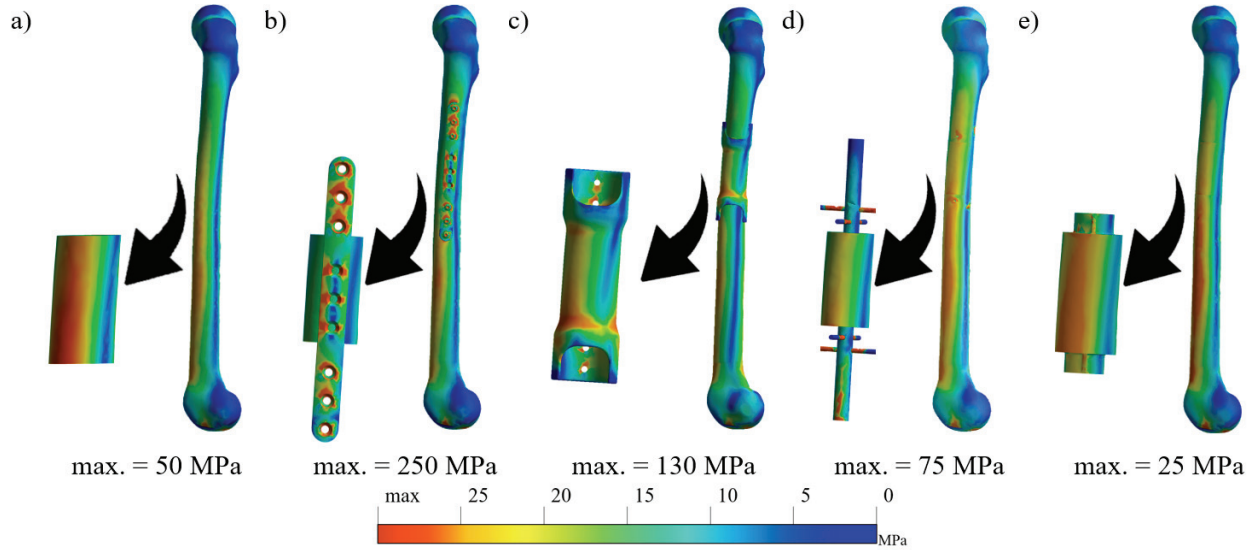

Fig. S1. HMH stress distribution for 20% of the gait cycle in lateral view: a) intact femur, b) method 1 – locking plate, c) method 2 – outer ring, d) method 3 – intramedullary nail, e) method 4 – double anti-rotation wedge

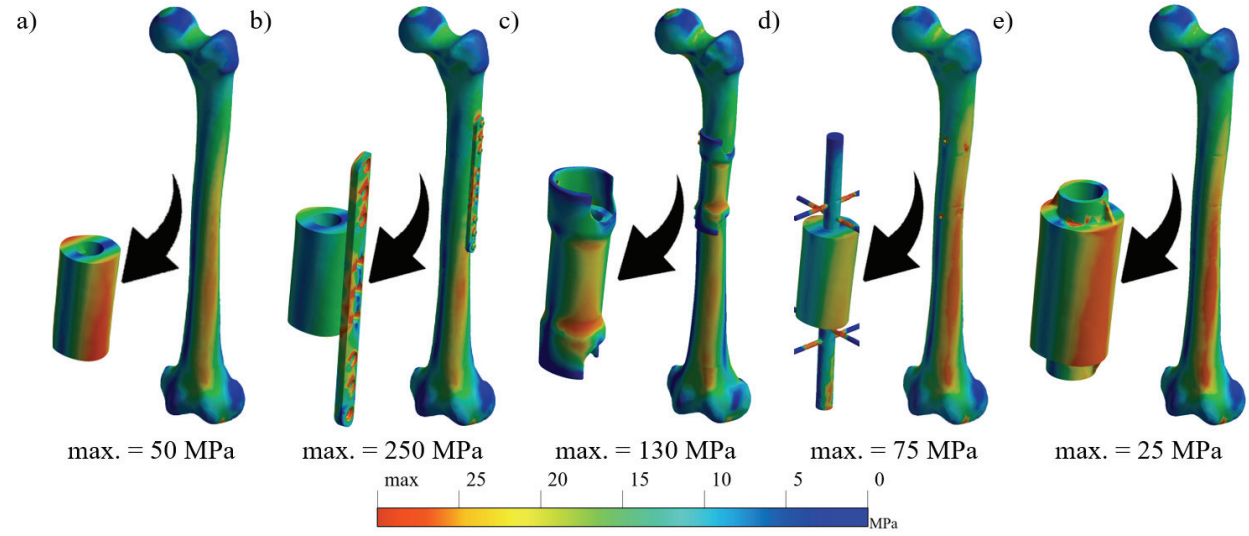

Fig. S2. HMH stress distribution for 20% of the gait cycle in isometric view: a) intact femur, b) method 1 – locking plate, c) method 2 – outer ring, d) method 3 – intramedullary nail, e) method 4 – double anti-rotation wedge

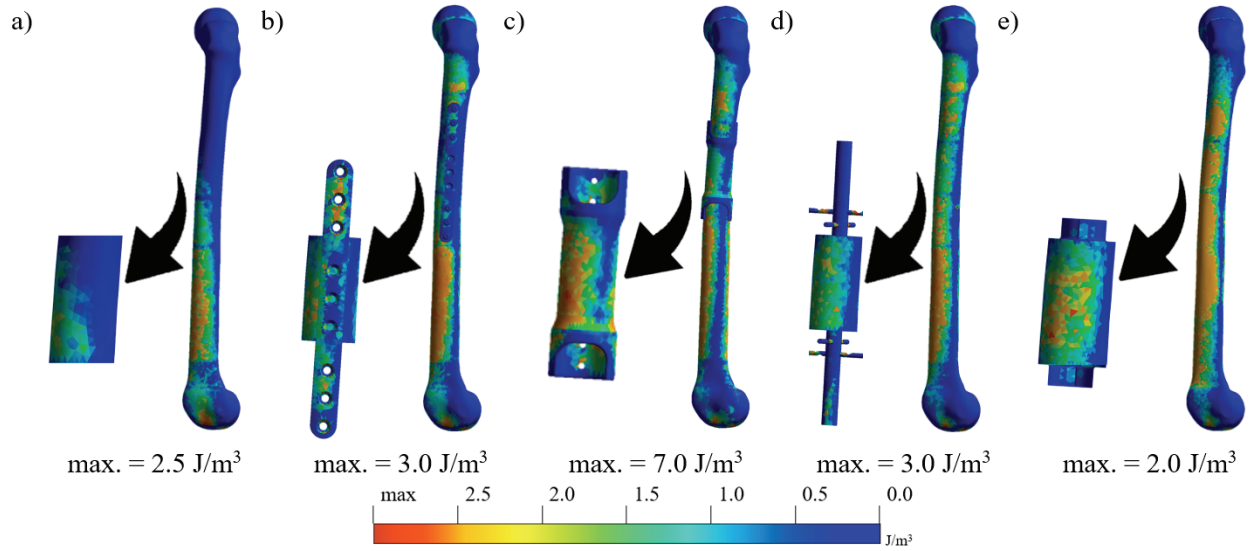

Fig. S3. SED distribution in lateral view: a) intact femur, b) method 1 – locking plate, c) method 2 – outer ring, d) method 3 – intramedullary nail, e) method 4 – double anti-rotation wedge

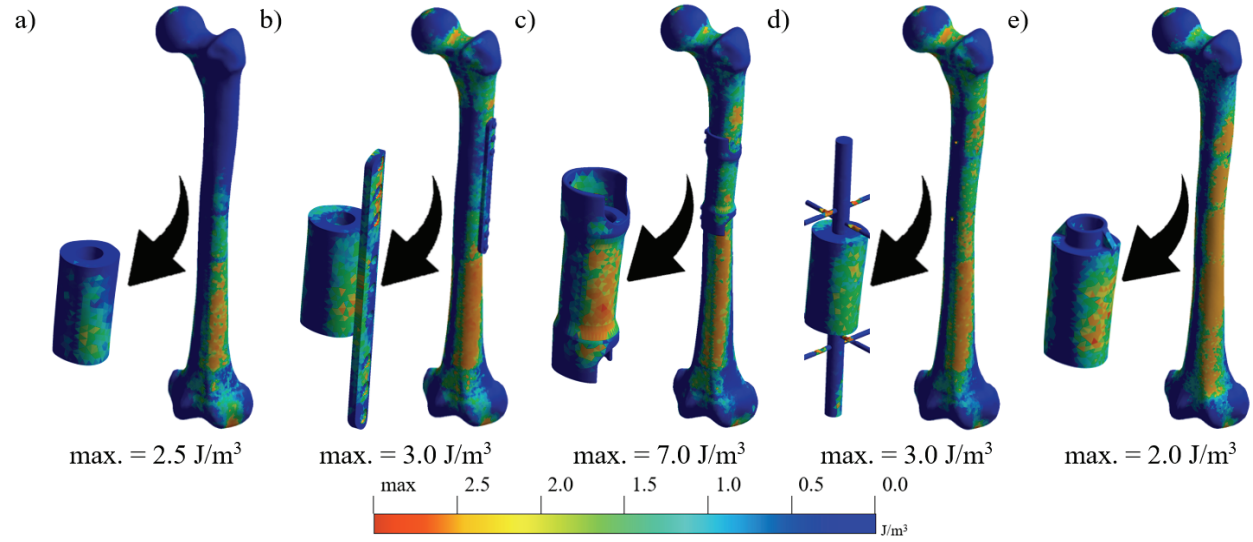

Fig. S4. SED distribution in isometric view: a) intact femur, b) method 1 – locking plate, c) method 2 – outer ring, d) method 3 – intramedullary nail, e) method 4 – double anti-rotation wedge